Dual Functional Roles of ATP in the Human Mitochondrial Malic Enzyme†

Wen-Chi Hsu,‡ Hui-Chih Hung,§ Liang Tong,|| and Gu-Gang Chang*,‡

Faculty of Life Sciences, Institute of Biochemistry, Structure Biology Program, and Proteome Research Center, National Yang-Ming University, Taipei 112, Taiwan, Department of Life Sciences, National Chung-Hsing University, Taichung 400, Taiwan, and Department of Biological Science, Columbia University, New York, New York 10027

Received February 26, 2004; Revised Manuscript Received April 19, 2004

ABSTRACT: Human mitochondrial malic enzyme is a regulatory enzyme with ATP as an inhibitor. Structural studies reveal that the enzyme has two ATP-binding sites, one at the NAD^+-binding site in the active center and the other at the exo site in the tetramer interface. Inhibition of the enzyme activity is due to the competition between ATP and NAD^+ for the nucleotide-binding site at the active center with an inhibition constant of 81 μM. Binding of the ATP molecule at the exo site, on the other hand, is important for the maintenance of the quaternary structural integrity. The enzyme exists in solution at neutral pH and at equilibrium of the dimer and tetramer with a dissociation constant (K_{TD}) of 0.67 μM. ATP, at a physiological concentration, shifts the equilibrium toward tetramer and decreases the K_{TD} by many orders of magnitude. Mutation of a single residue Arg542 at the tetrameric interfacial exo site resulted in dimeric mutants. ATP thus has dual functional roles in the mitochondrial malic enzyme.

Malic enzymes constitute a new class of oxidative decarboxylases with highly conserved amino acid sequences and similar overall structural topology among different species (*1*−*3*; see ref *4* for a review). In mammals, the mitochondrial $NAD(P)^+$-dependent malic enzyme is involved in the energy metabolism of neurons and fast-growing tissues (*5*−*7*). The enzyme could thus be an ideal target for the rational drug design with a potential application in anticancer chemotherapy.

The enzyme has a complex regulatory control system for the catalytic activity. ATP inhibits (*8*) while fumarate activates the enzymatic activity (*8*, *9*). The recent resolved crystal structures indicated that ATP and fumarate occupied the tetramer and dimer interfaces, respectively (Figure 1) (*10*). These results seem to provide a structural basis for the allosteric nature of ATP and fumarate in modulating the enzyme activity (*1*, *10*). This is true for the fumarate activation. However, a second ATP was also found at the NAD^+ site of the active center (*10*) and a NAD^+ was previously identified at the exo site in the open form of the enzyme (*1*). These structural features are unique for the human malic enzyme. The functional roles of the respective ATP in these two nucleotide-binding sites need to be clarified.

The double-dimer quaternary structure of pigeon cytosolic malic enzyme has many biochemical supporting evidences (*11*−*13*). However, little support has been found for the oligomerization state of the human malic enzyme in solution. One of the novel aspects of the present paper is that we provide experimental evidence supporting the involvement of the exo site ATP in the subunit association of human mitochondrial malic enzyme. Moreover, the inhibition of human malic enzyme by ATP is due to the competing of ATP with NAD^+ at the nucleotide-binding site of the active center.

EXPERIMENTAL PROCEDURES

Enzyme Mutagenesis and Purification. The full-length human mitochondrial malic enzyme cDNA was cloned in the pET21b vector as previously described for the pigeon liver malic enzyme (*14*). This construct yielded the malic enzyme protein without any extra tagged amino acid residues at the N terminus. Site-directed mutagenesis was carried out according to the procedures of Kunkel et al. (*15*). Malic enzyme mutants were produced using the Mutagene Phagemid Mutagenesis kit (BioRad). The primers used were 5′-CGGCCTGAT**GCA**TGCCTGCCA-3′ for R197A, 5′-CGGCCTGAT**GAA**TGCCTGCCA-3′ for R197E, 5′-ATGGCTTTC**GCA**TACCCAGA-3′ for R542A, and 5′-ATGGCTTTC**GAA**TACCCAGA-3′ for R542E, in which the mutation positions were underlined in bold face. Plasmid constructs were sequenced to confirm the presence of the mutations. The entire cDNA was also sequenced to exclude any unexpected mutations resulting from in vitro DNA polymerase extension. The absence of adventitious base changes was verified in all recombinant malic enzymes.

The mutant and wild-type enzymes were purified as described (*16*) with a modification. Briefly, malic enzyme was overexpressed in *Escherichia coli* and purified by anion exchange and ATP affinity chromatography using Q-Sepharose and ATP-agarose columns (Amersham Biosciences), respectively. The modification to the described protocol is the omission of the gel-filtration step. The purified proteins were exchanged in a TMK buffer containing 50 mM Tris-

† This work was supported by the National Science Council, ROC (NSC 92-2320-B-010-065 and NSC 92-2320-B-010-056 to G.G.C.). A preliminary report had been presented at the 48th Annual Meeting of the Biophysical Society held at Baltimore MD, U.S.A. on February 14-18, 2004.

* To whom correspondence should be addressed. Tel.: 886-2-2826-7000 (5530). Fax: 886-2-2820-2449. E-mail: ggchang@ym.edu.tw.

‡ National Yang-Ming University.

§ National Chung-Hsing University.

|| Columbia University.

10.1021/bi049600r CCC: $27.50
Published on Web 05/21/2004

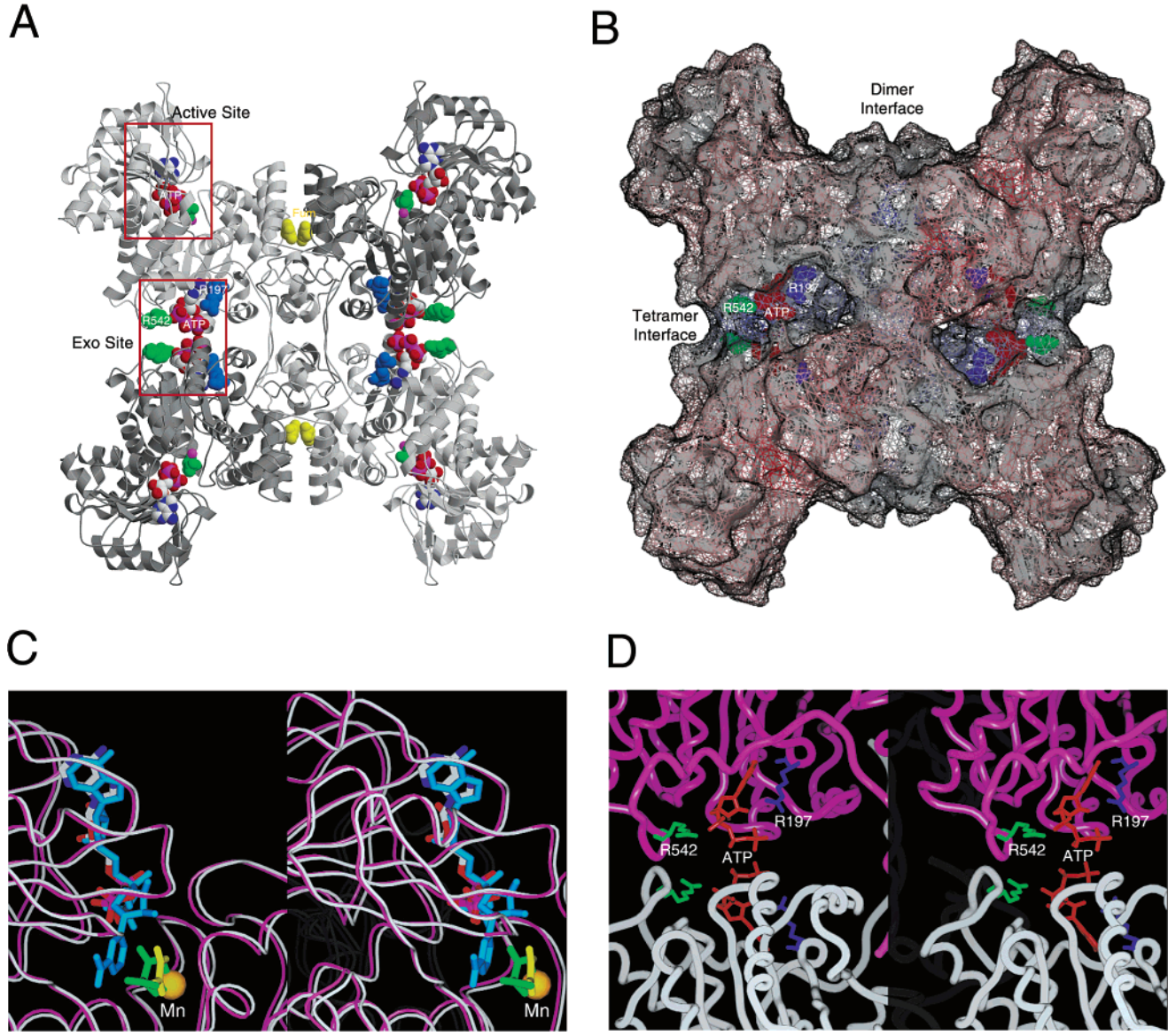

FIGURE 1: Crystal structure of the human mitochondrial malic enzyme. The enzyme in complex with ATP, tartronate, Mn^{2+}, fumarate (pdb code 1GZ4) was shown in ribbon (A) and surface (B) drawings. The active- and exo-site regions were highlight with red boxes, which were enlarged in C and D, respectively. The color code for atoms in A and B is CPK for ATP, green for tartronate, and magenta for Mn^{2+} in the active site, yellow for fumarate in the dimer interface, red for ATP, green for Arg542, and blue for Arg197 in the exo site. (C) Stereoview of the superimposition of 1GZ4 (violet) with the closed-form human malic enzyme (white) (pdb code 1DO8) at the active-site region. The superimposition of ATP (CPK) and NAD^+ (blue) is obvious. (D) Stereoview of the exo site at the tetramer interface. The worm color code is violet for subunit A and white for subunit D. A was generated with Molscript (*30*) and Raster3D (*31*).

HCl (pH 7.4), 10 mM $MnCl_2$, and 200 mM KCl. All purified enzymes were subjected to sodium dodecyl sulfate−polyacrylamide gel electrophoresis (SDS−PAGE) and analytical ultracentrifugation analyses to examine the purity.

Enzyme Assay. The reactant concentrations were corrected for the chelation with Mn^{2+} assuming a dissociation constant of 20 mM for the Mn^{2+}−L-malate (*17*), 12.9 mM for the Mn^{2+}−NAD^+ (*18*), and 100 mM for the Mn^{2+}−fumarate complexes (*19*).

Malic enzyme activity was assayed according to the published procedure (*20*). A 1-mL assay mixture contains the following components: 30 mM Tris-HCl (pH 7.4), 15 mM L-malate (pH 7.4) (14.3 mM when corrected for Mn^{2+}−L-malate chelation), 1 mM NAD^+ (0.94 mM when corrected for Mn^{2+}−NAD^+ chelation), 2 mM $MnCl_2$ (1.95 mM when corrected for Mn^{2+}−L-malate, Mn^{2+}−NAD^+, and Mn^{2+}−fumarate chelations), 2 mM fumarate (pH 7.4) (−2.0 mM when corrected for Mn^{2+}−fumarate chelation), and an appropriate amount of malic enzyme. The absorbance of the solution at 340 nm was monitored continuously with Perkin−Elmer Lambda-40 spectrophotometer at 30 °C. Apparent Michaelis constants for the substrate and cofactors were determined by varying the concentration of one substrate (or cofactors) around its K_m value, while maintaining other components at constant concentrations as stated above. These concentrations were at saturating levels even after correcting for the metal chelations.

The inhibition experiment of malic enzyme activity by ATP was performed at various ATP concentrations in different concentrations of the variable substrate ([*S*]). The free ATP concentration was calculated assuming a value of 0.01 mM for the dissociation constant of the Mn^{2+}−ATP complex (*21*). In the presence of ATP, the chelations by the substrate or cofactors are negligible. The whole set of data

Table 1: Kinetic Parameters for the Wild-Type and Exo-Site Mutant Human Mitochondrial Malic Enzymes

	$K_{m,Mn(app)}$ (μM)	$K_{m,Mal(app)}$ (mM)	$K_{m,NAD(app)}$ (μM)	k_{cat} (s^{-1})	$K_{i,ATP(free)}$ (μM) (to NAD^+)	$K_{i,ATP(free)}$ (μM) (to malate)
wild type	6.4 ± 0.6	1.4 ± 0.09	130 ± 8	26 ± 0.6	81 ± 8	474 ± 31
R197A	4.6 ± 0.2	1.2 ± 0.04	130 ± 5	49 ± 0.7	121 ± 20	393 ± 53
R197E	42 ± 3	2.2 ± 0.07	179 ± 5	52 ± 2.9	249 ± 21	252 ± 30
R542A	57 ± 2	1.7 ± 0.01	243 ± 14	52 ± 2.1	106 ± 7	294 ± 17
R542E	105 ± 4	1.1 ± 0.04	204 ± 18	11 ± 0.2	147 ± 16	382 ± 29

were analyzed by the following equation, which describes a competitive-inhibition pattern,

$$v = \frac{k_{cat}[E_0][S]}{[S] + K_m\left(1 + \frac{[ATP]_f}{K_{i,ATP(free)}}\right)}$$

in which v is the observed reaction rate, k_{cat} is the turnover number of the enzyme, $[E_0]$ is the total enzyme concentration, K_m is the Michaelis constant for the substrate, and $K_{i,ATP(free)}$ is the inhibition constant for free ATP. The inhibition pattern was presented as the double reciprocal plot.

The kinetic parameters were obtained by fitting the experimental data to appropriate kinetic models. The calculation was carried out with Sigma Plot 5.0 (Jandel, San Rafael, CA).

Characterization of Recombinant Human Malic Enzyme by Circular Dichroism (CD). The CD[1] measurements were made with a Jasco J-810 spectropolarimeter using a 0.1-cm path length cell under a constant N_2 flush. Three repetitive scans between 250 and 200 nm were averaged. Parallel spectra of a buffer solution without protein were also recorded and subtracted from the sample spectra. Mean residue ellipticity (Φ) was calculated by the following equation:

$$\Phi = \frac{[\Phi]_{222} M_{MRW}}{10dc}$$

in which the weight of the mean amino acid residue, M_{MRW}, is 111.42. d is the cell path in centimeters, and c is the enzyme concentration in milligrams per milliliter.

Sedimentation Velocity Analysis. Sedimentation velocity experiments were performed with a Beckman XL-A ultracentrifuge in an An60Ti or An50Ti rotor at 20 °C and 40 000 rpm. Enzyme samples were diluted to concentrations between 0.125 and 1.0 mg/mL and loaded into 2-sector cells with aluminum or epon centerpieces, and absorbance data at 280 nm were collected in continuous mode every 5 min for a period of 2.5 h. Data were analyzed with SEDFIT using the c(S) or c(M) Lamm equation model (*22*−*24*). Collections of 10−30 radial scans were used for analysis, and 200 sedimentation coefficients between 1.8 and 20 S were employed in calculating the c(S) or c(M) distribution. The position of the meniscus and cell bottom were determined by visual inspection and then refined in the final fit. The partial specific volume for the wild-type and mutant enzymes was calculated to be 0.7403 mL/g as determined from the wild-type sequence. The solvent density and viscosity were corrected with the ULTRASCAN version 5.0 (*25*). All samples were visually checked for clarity after ultracentrifugation.

[1] Abbreviation: CD, circular dichroism.

To determine the equilibrium constant between the oligomers, the sedimentation velocity data were global fitted with SEDFIT. A monomer−dimer−tetramer equilibrium system gives a better fitting result than the tetramer−dimer system. However, the monomer amount was small, and thus only the dissociation constant for the tetramer−dimer equilibrium was reported in this paper.

RESULTS

Characterization of the Recombinant Human Malic Enzymes. All recombinant malic enzymes were successfully expressed and purified to homogeneity (data not shown). ATP-agarose affinity chromatography is an effective purification step. This also applies to the point mutants at Arg197 or Arg542.

The kinetic parameters of the recombinant human malic enzymes were shown in Table 1. All those values were determined in the presence of 2 mM fumarate, which decrease the $K_{m,Mn(app)}$, $K_{m,NAD(app)}$, and $K_{m,Mal(app)}$ values by 9.2-, 1.2-, and 1.3-fold, respectively. The k_{cat} was increased by 13% with fumarate.

The purified enzymes show almost identical CD spectra from 200 to 250 nm (not shown). When excited with 280 nm of UV light, the fluorescence emission spectra of all recombinant malic enzymes are identical (not shown). The secondary and tertiary structures of the recombinant enzyme are essentially the same for all mutants. The quaternary structure of various mutants, as anticipated, was quite different from that of the wild type (see below).

Inhibition of Human Malic Enzyme by ATP. Human malic enzyme is strongly inhibited by ATP. Because the structural studies do not indicate a second metal site in the presence of ATP, free ATP was assumed to be the inhibiting species. The ATP concentration was thus corrected for the Mn^{2+}−ATP complex. A double-reciprocal plot of the inhibition pattern gives an intercepting pattern with all lines intercepted at the y axis (Figure 2), yielding $K_{i,ATP(free)}$ values of 81 ± 8 and 474 ± 31 μM with respect to NAD^+ and malate, respectively, indicating a simple competitive-inhibition pattern in both cases. Structural studies indicate that ATP is bound at the NAD-binding site, occupying the adenosine diphosphate binding region (Figure 1C). The inhibition is thus due to the competition of ATP with the catalytic nucleotide-binding site.

The crystal structure of the enzyme indicates that, besides an ATP molecule found at the active site, another ATP was bound at the exo site, located at the tetramer interface (Figure 1D). The physiological implication of an ATP molecule at the exo site is not clear. Because it is located at the tetramer interface, we checked the effect of ATP binding at this site on the quaternary structure of the enzyme.

Quaternary Structure of the Human Mitochondrial Malic Enzyme. The aggregation states of the purified wild-type

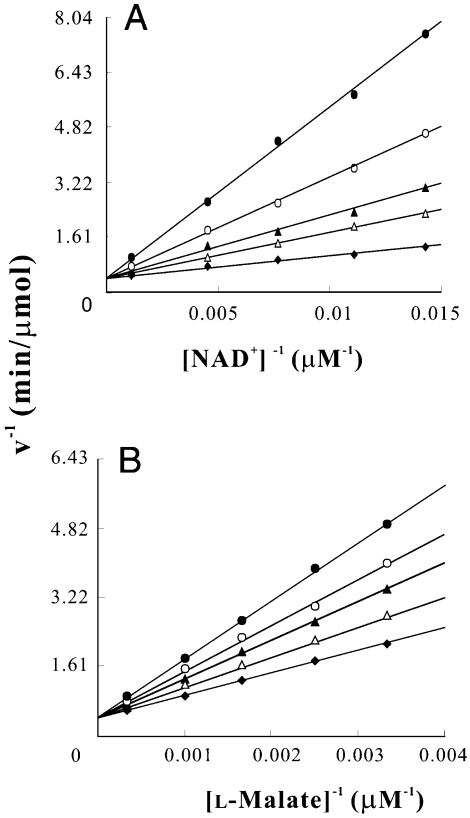

FIGURE 2: Competitive inhibition of the human mitochondrial malic enzyme by ATP with respect to NAD^+ and L-malate. Malic enzyme activity was measured at different concentrations of NAD^+ (A) or L-malate (B) at various concentrations of free ATP (from top to bottom, the chelation-corrected free ATP concentrations were 654, 260, 117, 44, and 0 μM in A and 864, 447, 260, 117, and 0 μM in B).

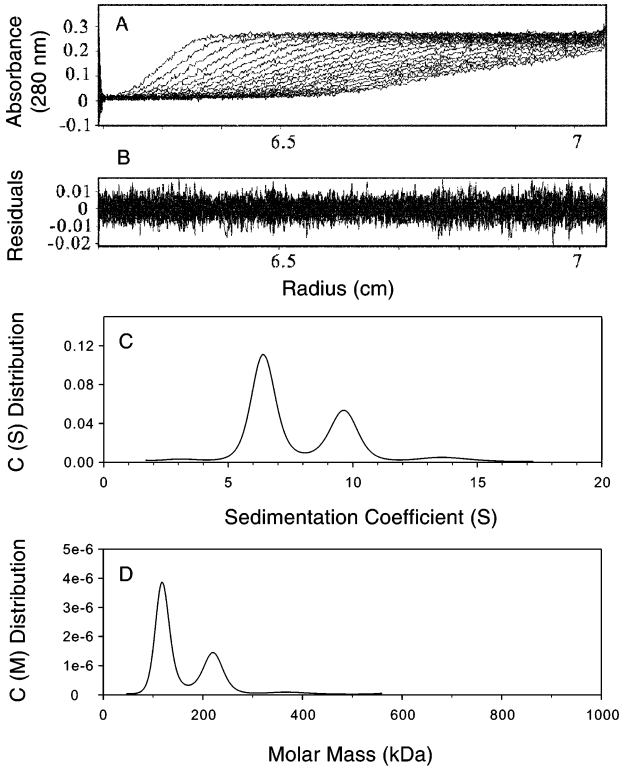

FIGURE 3: Sedimentation velocity analysis of the recombinant human mitochondrial malic enzyme. (A) Optical traces of the wild-type enzyme during ultracentrifugation. These traces were fitted to the Lamm equation by SEDFIT, and B shows the fitting residuals. The fitting residuals were randomly distributed. The distribution of the tetramer and dimer of the enzyme at a protein concentration of 0.3 mg/mL was analyzed by sedimentation velocity. (C) Continuous sedimentation coefficient distribution. (D) Continuous molar mass distribution.

malic enzyme were evaluated in sedimentation velocity experiments (Figure 3). Analysis of the sedimentation data with SEDFIT (*22*−*24*) resulted in high-quality-data fits with randomly distributed residuals and root-mean-square deviations below 0.1% (Figure 3B). The calculated sedimentation coefficient distributions revealed well-resolved peaks corresponding to the different aggregation states of the enzyme (Figure 3C). The wild-type enzyme exists primarily as a tetramer and a dimer in solution. The major peak at 9.4 S agrees well with previous hydrodynamic measurements for the pigeon enzyme (*12*, *13*). A second peak appears at 6.5 S and corresponds to the dimer form (parts C and D of Figure 3). According to the integrated distribution area, the dimer and tetramer accounted for 83 and 15% of the species present, respectively, at a protein concentration of 0.3 mg/mL. The remaining area in this and other distributions are likely contributions from monomers or from an error in the data fit. Different enzyme preparations do give slightly different proportions between the different aggregation forms. However, the effects of various factors that influence the distribution were always reproducible and more significant (see below).

The distribution between the tetramer and dimer varies depending on the protein concentration. A higher protein concentration favors tetramer formation but decreases the dimer amount (Figure 4). The close correlation between the two peaks with protein concentration indicates that an equilibrium dimer−tetramer system exists in solution.

Global fitting of the sedimentation data with SEDFIT obtained a dissociation constant (K_{TD}) of 0.67 μM for the tetramer−dimer equilibrium system.

Effect of ATP on the Dimer−*Tetramer Equilibrium of Human Malic Enzyme.* Malic enzyme had a double-dimer quaternary structure with the dimer interface more intimately interacting than the tetramer interface (*4*). Because an ATP molecule is bound at the exo site of the tetramer interface, we then checked the effect of ATP on the quaternary structure of the enzyme. Figure 5 showed that ATP induced tetramer formation. The dissociation constant for the tetramer−dimer equilibrium decreased to 3.12×10^{-6} or 1.51×10^{-12} μM in the presence of 0.5 or 1.5 mM ATP, respectively. This establishes the functional role of the ATP at the exo site.

We have also tested the effect of NAD^+ on the quaternary structure of the human malic enzyme. The effect of a small concentration of NAD^+ is not obvious. At large NAD^+ concentrations, however, the high UV absorption background precludes a reliable determination from the analytical ultracentrifuge based on UV absorption. NAD^+ may compete with ATP for the exo site albeit with lower affinity than ATP. Under the conditions that allow formation of crystals, the local NAD^+ concentration may be very high and forces the NAD^+ to bind to the exo site.

Because adding ATP into the enzyme solution also introduces ionic strength of the system, we checked the effect of NaCl on the quaternary structure of human malic enzyme.

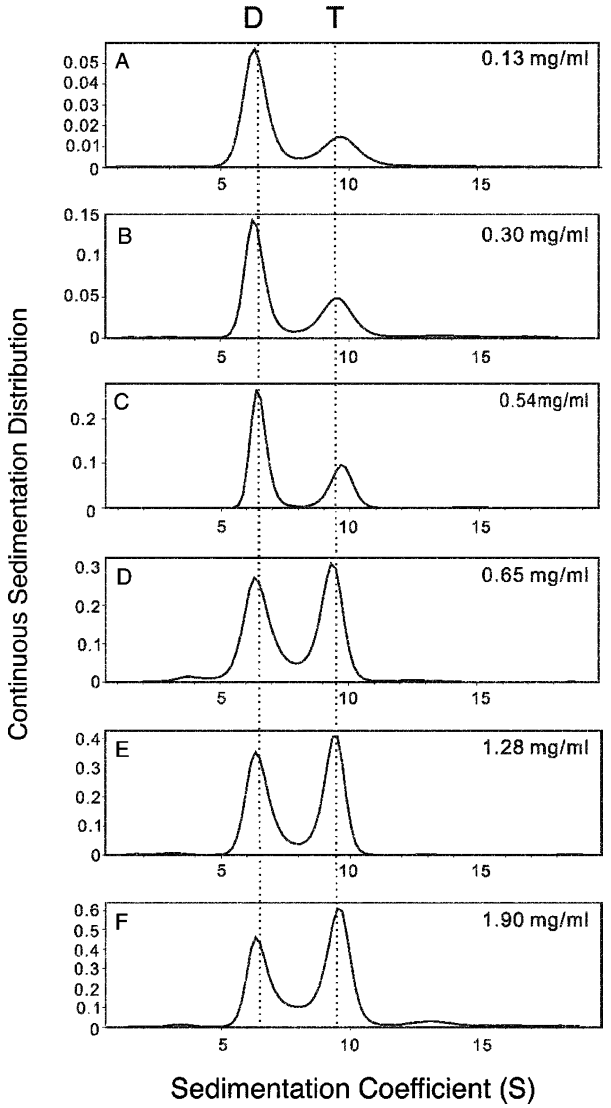

FIGURE 4: Effect of the protein concentration on the quaternary structure of the human malic enzyme. The distribution of the tetramer and dimer of the enzyme at various protein concentrations was analyzed by sedimentation velocity.

The data shown in Figure 6 indicated that at very high NaCl concentrations, the dimer−tetramer distribution seemed to be disturbed. However, the major effect was on the enzyme conformation. The enzyme became looser as indicated by the smaller sedimentation coefficient.

To confirm the role of exo ATP, several putative ATP-binding ligands at the exo site were mutated and the mutant malic enzymes were expressed, purified, and analyzed with analytical ultracentrifugation to examine the effect of mutation at interfacial residues on the subunit association.

Arg197 and Arg542 Mutations Disrupt the Tetramer Interface. To design mutants that perturb the stability of the tetramer of malic enzyme, the tetramer interfaces in the crystal structure were examined for residues in close proximity with atoms from an ATP molecule. Two arginyl residues, Arg197 and Arg542, which have charge or hydrogen-bonding interactions with the α phosphate or the 2′-hydroxy group of ATP were selected as the targets. Four point-mutant malic enzyme constructs were produced. All of these mutants were purified to homogeneity and evaluated by analytical ultracentrifugation.

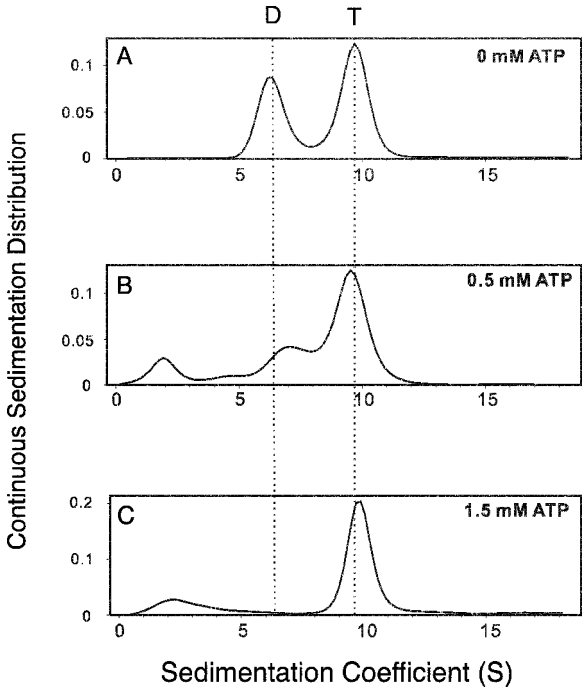

FIGURE 5: Effect of ATP on the quaternary structure of the human malic enzyme. The distribution of the tetramer, dimer, and monomer of the wild-type malic enzyme (0.3 mg/mL) in the presence of various ATP concentrations was analyzed by sedimentation velocity.

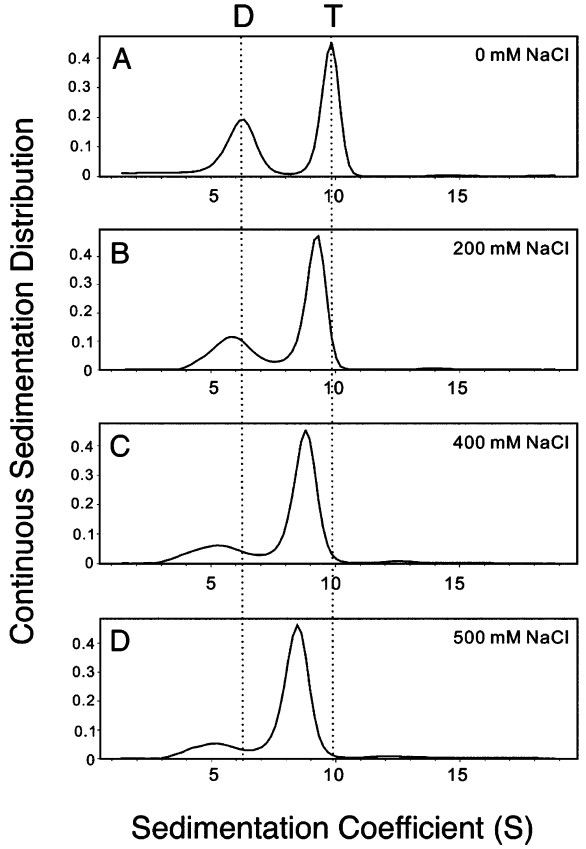

FIGURE 6: Effect of NaCl on the quaternary structure of the human malic enzyme. The distribution of the tetramer and dimer of the wild-type enzyme (1.0 mg/mL) at various NaCl concentrations was analyzed by the sedimentation velocity.

Mutation at Arg197 or Arg542 did not have a noticeable affect on the kinetic parameters of the mutants (Table 1). All mutants had similar k_{cat} with the wild type, except R542E,

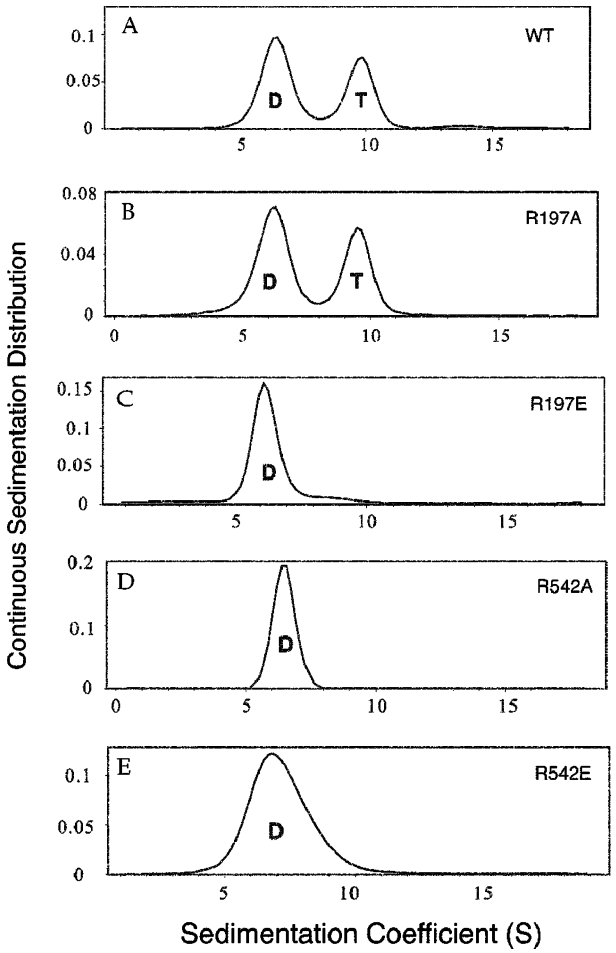

FIGURE 7: Continuous sedimentation coefficient distribution of the wild type and various mutants. Sedimentation velocity analyses of the wild-type and various mutant malic enzymes: (A) wild type, (B) R197A, (C) R197E, (D) R542A, and (E) R542E. All enzyme preparations used have a concentration of 0.3 mg/mL.

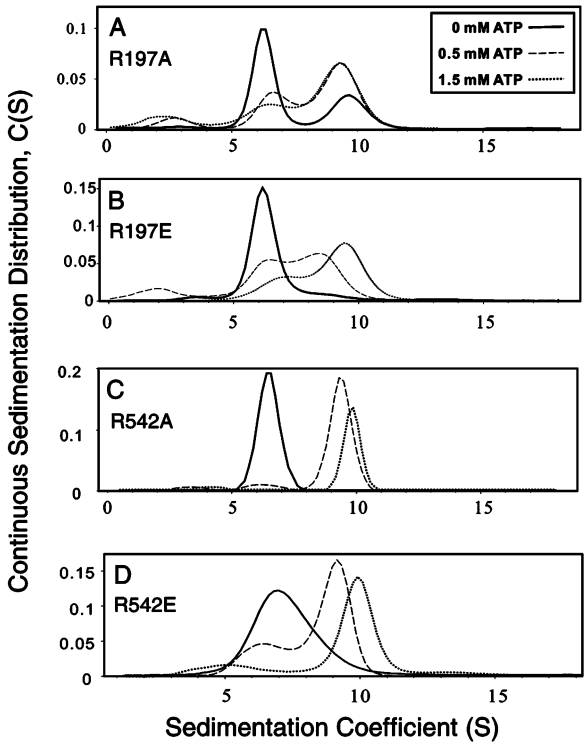

FIGURE 8: Effect of ATP on the quaternary structure of the mutant human malic enzymes. The distribution of the tetramer, dimer, and monomer of the mutant malic enzymes (all in 0.3 mg/mL) in the presence of various ATP concentrations was analyzed by sedimentation velocity. (A) R197A, (B) R197E, (C) R542A, and (D) R542E.

which is only one-third as active compared with the wild type. ATP competitively inhibited all mutants, either to NAD^+ or to malate (Table 1), in the presence of fumarate or in the absence of fumarate (not shown). Thus, the active-site region is not affected by the mutation at the exo site. The effect of mutation on the quaternary structure was then examined by analytical ultracentrifugation.

Mutation of Arg197 to alanine did not affect the tetramer−dimer distribution (Figure 7B), while mutation of the same residue to glutamate resulted in complete dissociation of the tetramer to the dimer (Figure 7C). Mutation of Arg542, whether to alanine or glutamate, resulted in exclusive dimer formation (parts D and E of Figure 7).

The effect of ATP on the quaternary structure of the mutant malic enzymes was shown in Figure 8. Similar to the wild-type malic enzyme, ATP induced tetramer formation in all mutant enzymes. The most affected mutant is R542A, in which almost all enzyme molecules existed as tetramers in the presence of 1.5 mM ATP.

DISCUSSION

In the initial stage of the present research, the crystal structure of the enzyme in complex with ATP has not been solved. The selected mutation points were determined by the crystal structure of the NAD^+−enzyme binary complex, which reveals two NAD^+-binding sites. Besides the one at the active site as anticipated, there is another NAD^+ molecule bound at the tetramer interface (*1*). When the crystal structure of the enzyme−ATP−Mn^{2+}−tartronate−fumarate complex was solved (*10*), it also revealed two ATP-binding sites, at exactly the same positions as NAD^+ was located, superimposed onto the adenosine diphosphate moiety of NAD^+ (Figure 1C). It becomes clear that ATP and NAD^+ are competing for the same active and exo sites, which explains the competitive-inhibition nature of ATP with respect to NAD^+ (Figure 2A).

The competitive-inhibition pattern observed for ATP with respect to L-malate is not conceivable or straightforward. ATP is not structurally related to L-malate, and their binding sites in the active center are not overlapping. Monod et al. (*26*) had predicted a similar kinetic situation for an allosteric inhibitor if either the inhibitor or the substrate induces a conformational change that prevents the binding of the other. Analogous to this, if ATP or L-malate induces a conformational change, which prevents the binding of the other, a result like that shown in Figure 2 will be obtained (*26*, *27*). For human malic enzyme, structural studies indicate that the enzyme−NAD^+ binary complex assumes an open-form structure (*1*, *4*) and the enzyme transforms to a closed-form structure in the presence of the substrate L-malate (*4*, *10*). It seems that ATP binding to the active site of the closed form is hindered because of the closure of the active site, and thus we observed the competitive-inhibition pattern.

A triple mutant R(197/542/556)A with abolished ATP binding at the exo site cannot be adsorbed to the ATP-affinity column (*10*). Attempts to purify the R(197/542/556)A triple mutant by other purification methods was not successful. It

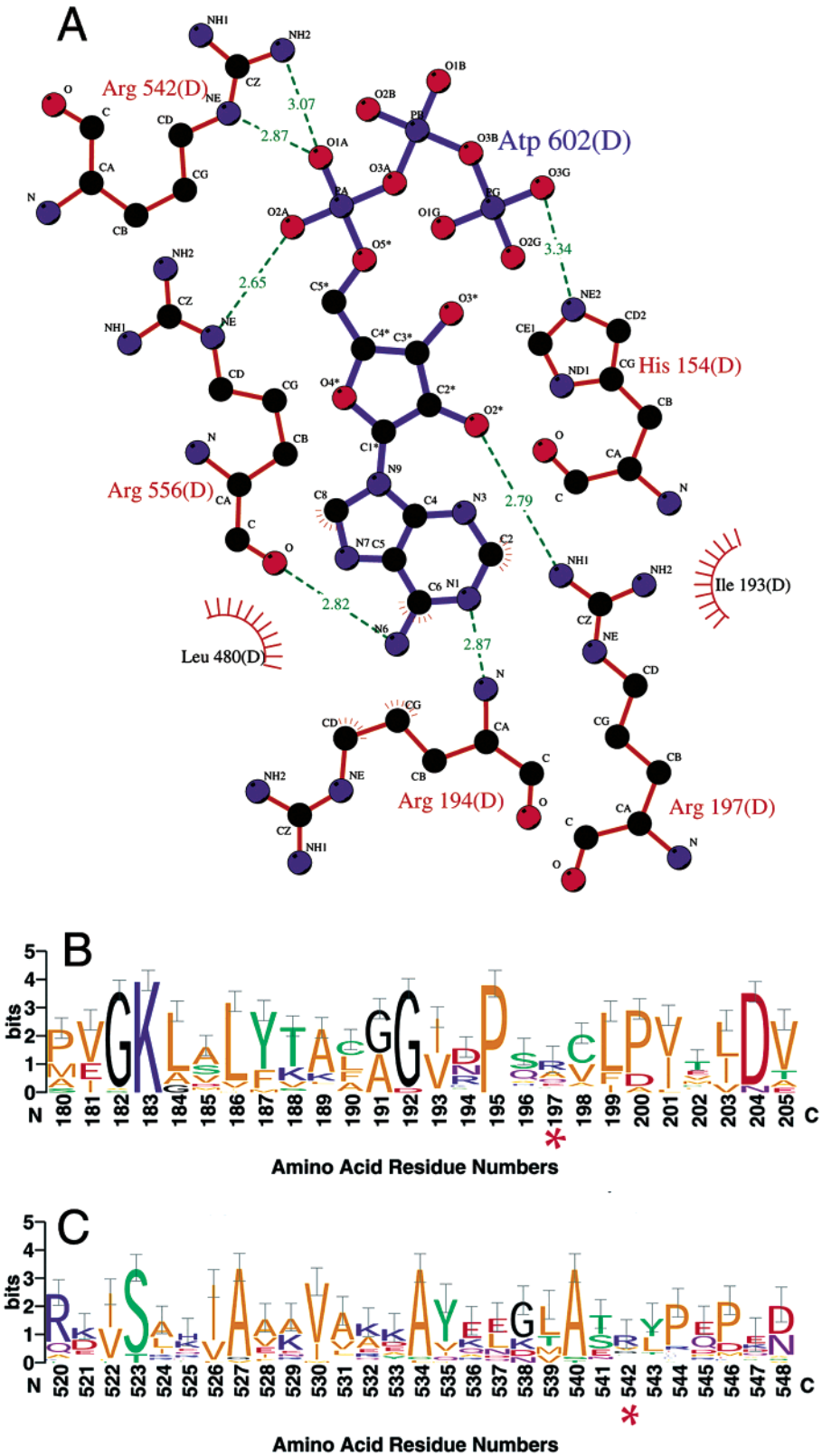

FIGURE 9: LIGPLOT and sequence logos of the exo site of the human malic enzyme. (A) LIGPLOT diagram (*32*). The bold bonds belong to the ATP, the thin bonds belong to the hydrogen-bonded residues from the enzyme, and the dashed lines represent the hydrogen bonds. Spoked arcs represent hydrophobic contacts. (B and C) Sequence logos around the exo site of the 37 malic enzymes with amino acid sequences available. Amino acid sequences of malic enzymes were searched for alignment by the ConSurf (*33*), and the results are expressed by sequence logos with error bars shown (*34*). The mutation points are highlighted with red stars. In B and C, the color codes for the amino acids are blue for basic residues (Lys, Arg, and His), red for acidic residues (Asp and Glu), violet for amide residues (Asn and Gln), green for other neutral/polar residues, and orange for hydrophobic residues.

is not possible to test the quaternary structure of this mutant enzyme. However, ATP still competitively inhibited this mutant and other exo site mutants (*10*) (Table 1). It is clear that the ATP-affinity column is determined by the ATP-

binding affinity to the exo site and not to the active site predicted by Moreadith and Lehninger (*28*). It also indicates that the inhibition of human malic enzyme by ATP is not due to allosteric inhibition but competition of ATP with the NAD^+ at the active site. The regulation of the human mitochondrial malic enzyme by feedback inhibition of ATP is consistent with the physiological role of the enzyme in the metabolism of glutamine for energy production (*4*−*8*).

Novel findings of the present investigation included that mutations at the exo ATP site of the human malic enzyme affect the tetramer interface and produce dimers, which presumably have an intact dimer interface. Excess ATP, however, can restore the tetrameric structure in wild-type and mutant enzymes (Figures 5 and 8). This is understandable because ATP bound at the exo site involves multiple points. Mutation at a single point will not abolish the binding energy. It is clear that the ATP at the exo site is essential for the quaternary structural integrity of the human malic enzyme. This establishes the important functional role of the exo site of the human enzyme. However, in the presence of ATP, significant amounts of species with small *S* values were also detected. Because the enzyme preparation was homogeneous, this small peak was assumed to be the monomer. Global fitting of the sedimentation data also indicated a better result with the tetramer−dimer−monomer system rather than the tetramer−dimer system in these cases (Figures 5 and 8).

Analysis of the crystal structures reveals that there are substantial differences between the human mitochondrial and pigeon cytosolic malic enzymes at the subunit interfaces (*4*). Figure 9A shows the LIGPLOT of the ATP-binding mode at the exo site of the human enzyme. The major interactions between Arg197 and Arg542 and ATP are hydrogen bonds. Although there are many amino acids (His154, Arg194, Arg197, Arg542, and Arg556) involved in the ATP binding, mutation at a single point, Arg542, is enough to produce exclusively dimeric mutants. The two hydrogen bonds between the α-phosphate moiety of ATP and the guanidino group of Arg542 must play a major role in ATP binding to the exo site. The R197A mutant has an almost identical dimer−tetramer distribution compared to the wild type, indicating that the hydrogen bond between Arg197 and the ribosyl 2′-hydroxy group of ATP plays a less-important role in the aggregation state of the enzyme. We have also prepared some Arg556 mutants. These mutants also have similar kinetic parameters as the wild type (data not shown). However, these mutants bind to the ATP-affinity column poorly; further, gel-filtration step is necessary for their purification. These mutants are less-satisfactory in the final purity. Although Arg556 may also play an important role in the ATP binding at the exo site, no further attempt was made to characterize their involvement in the quaternary structure.

The aligned sequence logos of the exo site around Arg197 and Arg542 clearly indicate that this region is not conserved among malic enzymes from various sources (Figure 9B). From this figure it is clear that, besides the putative hydrogen bonds, the subunit association at the tetramer interface involves hydrophobic interactions as the major force (orange-colored residues in parts B and C of Figure 9). The pigeon malic enzyme exists exclusively as a tetramer in neutral solution (*11*, *12*, *29*). Under identical conditions, the human enzyme exists as a mixture of the dimer and tetramer (Figure 3). ATP does not inhibit the pigeon cytosolic malic enzyme. Structural studies do not reveal an exo site for the pigeon cytosolic (*2*) or *Ascaris suum* mitochondrial malic enzyme (*3*). The functional role of the ATP at the exo site seems exclusively for the human mitochondrial malic enzyme.

From the above discussion, we reach two conclusions. First, the inhibition of human mitochondrial malic enzyme by ATP is due to the competition of ATP with the NAD^+ at the nucleotide-binding site of the active center. ATP is not an allosteric regulator of the enzyme. Second, the ATP molecule bound at the exo site is essential for the quaternary structural integrity of the enzyme. The ATP molecule bound at this site does not affect the enzyme activity. These two ATP sites do not have clear-cut affinity differences for the ligand. However, because half of the inhibition was held at 81 μM ATP, while the effect of ATP on the dimer association occurred at larger ATP concentrations, the active site seems to have slightly higher affinity with ATP than the exo site.

REFERENCES

1. Xu, Y., Bhargava, G., Wu, H., Loeber, G., and Tong, L. (1999) Crystal structure of human mitochondrial $NAD(P)^+$-dependent malic enzyme: A new class of oxidative decarboxylases, *Structure 7*, 877−889.
2. Yang, Z., Zhang, H., Hung, H. C., Kuo, C. C., Tsai, L. C., Yuan, H. S., Chou, W. Y., Chang, G. G., and Tong, L. (2002) Structural studies of the pigeon cytosolic NADP(+)-dependent malic enzyme, *Protein Sci. 11*, 332−341.
3. Coleman, D. E., Rao, G. S., Goldsmith, E. J., Cook, P. F., and Harris, B. G. (2002) Crystal structure of the malic enzyme from *Ascaris suum* complexed with nicotinamide adenine dinucleotide at 2.3 Å resolution, *Biochemistry 41*, 6928−6938.
4. Chang, G. G., and Tong, L. (2003) Structure and function of malic enzymes, a new class of oxidative decarboxylases, *Biochemistry 42*, 12721−12733.
5. Moreadith, R. W., and Lehninger, A. L. (1984) The pathways of glutamate and glutamine oxidation by tumor cell mitochondria. Role of mitochondrial $NAD(P)^+$-dependent malic enzyme, *J. Biol. Chem. 259*, 6215−6221.
6. Reitzer, L. J., Wice, B. M., and Kennell, D. (1979) Evidence that glutamine, not sugar, is the major energy source for cultured HeLa cells, *J. Biol. Chem. 254*, 2669−2676.
7. Teller, J. K., Fahien, L. A., and Davis, J. W. (1992) Kinetics and regulation of hepatoma mitochondrial NAD(P) malic enzyme, *J. Biol. Chem. 267*, 10423−10432.
8. Sauer, L. A. (1973) An NAD- and NADP-dependent malic enzyme with regulatory properties in rat liver and adrenal cortex mitochondrial fractions, *Biochem. Biophys. Res. Commun. 50*, 524−531.
9. Landsperger, W. J., and Harris, B. G. (1976) NAD^+−malic enzyme. Regulatory properties of the enzyme from *Ascaris suum*, *J. Biol. Chem. 251*, 3599−3602.
10. Yang, Z., Lanks, C. W., and Tong, L. (2002) Molecular mechanism for the regulation of human mitochondrial $NAD(P)^+$-dependent malic enzyme by ATP and fumarate, *Structure 10*, 951−960.
11. Chang, G. G., Huang, T. M., and Chang, T. C. (1988) Reversible dissociation of the catalytically active subunits of pigeon liver malic enzyme, *Biochem. J. 254*, 123−130.
12. Chang, H. C., Chou, W. Y., and Chang, G. G. (2002) Effect of metal binding on the structural stability of pigeon liver malic enzyme, *J. Biol. Chem. 277*, 4663−4671.
13. Chang, H. C., and Chang, G. G. (2003) Involvement of single residue tryptophan 548 in the quaternary structural stability of pigeon cytosolic malic enzyme, *J. Biol. Chem. 278*, 23996−24002.
14. Chou, W. Y., Huang, S. M., and Chang, G. G. (1997) Functional roles of the N-terminal amino acid residues in the Mn(II)−L-malate binding and subunit interactions of pigeon liver malic enzyme, *Protein Eng. 10*, 1205−1211.
15. Kunkel, T. A., Roberts, J. D., and Zakour, R. A. (1987) Rapid and efficient site-specific mutagenesis without phenotypic selection, *Methods Enzymol. 154*, 367−382.

16. Bhargava, G., Mui, S., Pav, S., Wu, H., Loeber, G., and Tong, L. (1999) Preliminary crystallographic studies of human mitochondrial NAD(P)(+)-dependent malic enzyme, *J. Struct. Biol. 127*, 72−75.
17. Hsu, R. Y., Mildvan, A. S., Chang, G. G., and Fung, C. H. (1976) Mechanism of malic enzyme from pigeon liver. Magnetic resonance and kinetic studies of the role of Mn^{2+}, *J. Biol. Chem. 251*, 6574−6583.
18. Gavva, S. R., Harris, B. G., Weiss, P. M., and Cook, P. F. (1991) Modification of a thiol at the active site of the *Ascaris suum* NAD−malic enzyme results in changes in the rate-determining steps for oxidative decarboxylation of L-malate, *Biochemistry 30*, 5764−5769.
19. Dawson, R. M. C., Elliott, D. C., Elliott, W. H., and Jones, K. M. (1986) *Data for Biochemical Research*, 3rd ed., p 411, Clarendon Press, Oxford, U.K.
20. Loeber, G., Dworkin, M. B., Infante, A., and Ahorn, H. (1994) Characterization of cytosolic malic enzyme in human tumor cells, *FEBS Lett. 344*, 181−186.
21. O'Sullivan, W. J., and Cohn, M. (1966) Magnetic resonance investigations of the metal complexes formed in the manganese-activated creatine kinase reaction, *J. Biol. Chem. 241*, 3104−3115.
22. Schuck, P. (2000) Size-distribution analysis of macromolecules by sedimentation velocity ultracentrifugation and Lamm equation modeling, *Biophys. J. 78*, 1606−1619.
23. Lebowitz, J., Lewis, M. S., and Schuck, P. (2002) Modern analytical ultracentrifugation in protein science: A tutorial review, *Protein Sci. 11*, 2067−2079.
24. Schuck, P. (2003) On the analysis of protein self-association by sedimentation velocity analytical ultracentrifugation, *Anal. Biochem. 320*, 104−124.
25. Demeler, B., and Saber, H. (1998) Determination of molecular parameters by fitting sedimentation data to finite-element solutions of the Lamm equation, *Biophys. J. 74*, 444−454.
26. Monod, J., Changeux, J. P., and Jacob, F. (1963) Allosteric proteins and cellular control systems, *J. Mol. Biol. 6*, 306−329.
27. Dixon, M., and Webb, E. C. (1979) *Enzymes*, 3rd ed., p 335, Academic Press, New York.
28. Moreadith, R. W., and Lehninger, A. L. (1984) Purification, kinetic behavior, and regulation of $NAD(P)^+$ malic enzyme of tumor mitochondria, *J. Biol. Chem. 259*, 6222−6227.
29. Huang, T, M., and Chang, G. G. (1992) Characterization of the tetramer−dimer−monomer equilibrium of the enzymatically active subunits of pigeon liver malic enzyme, *Biochemistry 31*, 12658−12664.
30. Kraulis, P. (1991) MOLSCRIPT: A program to produce both detailed and schematic plots of protein structures, *J. Appl. Crystallogr. 24*, 946−950.
31. Merritt, E. A., and Bacon, D. J. (1997) Raster3D: Photorealistic molecular graphics, *Methods Enzymol. 277*, 505−524.
32. Wallace, A. C., Laskowski, R. A., and Thornton, J. M. (1995) LIGPLOT: A program to generate schematic diagrams of protein−ligand interactions, *Protein Eng. 8*, 127−134.
33. Glaser, F., Pupko, T., Paz, I., Bell, R. E., Bechor-Shental, D., Martz, E., and Ben-Tal, N. (2003) ConSurf: Identification of functional regions in proteins by surface-mapping of phylogenetic information, *Bioinformatics 19*, 163−164.
34. Schneider, T. D., and Stephens, R. M. (1990) Sequence logos: A new way to display consensus sequences, *Nucleic Acids Res. 16*, 6097−6100.

BI049600R